Seismic Rehabilitation of Welded Steel Beam-to-Box Column Connections Utilizing Internal Flange Stiffeners

Chung-Che Chou[a] **and Chih-Kai Jao**[b]

This work investigates the seismic performance of rehabilitated steel moment connections using internal flange stiffeners (IFSs) welded to the face of a built-up box column and a beam flange inner side. The objective is to provide a rehabilitation scheme that excludes interference from the composite slab and story height limitation in an existing steel building. Five rehabilitated moment connections with different IFSs were tested according to AISC (2005) loading protocol to validate their cyclic performance. Two rehabilitated moment connections had excellent performance; no welded joint fractures were found in the connections with a drift in excess of 4%. The specimens were modeled using the computer program ABAQUS to further verify the effectiveness of the IFSs in transferring beam moments to a column and to investigate potential sources of connection failure. Design guidelines for the rehabilitation scheme are provided based on test and analytical results. [DOI: 10.1193/1.3480275]

INTRODUCTION

Widespread damage to welded steel moment connections by the 1994 Northridge earthquake and 1995 Hyogoken-Nanbu (Kobe) earthquake initiated research focused on improving the seismic performance of connections (Chou and Uang 2007, Chou et al. 2008). Prior to the Northridge earthquake, most moment connections in the United States had an H-shaped column cross section with beam flanges groove-welded to the column using AWS E70T-4 self-shielded, flux-cored wire. Use of this electrode, which has a very low Charpy V-notch (CVN) fracture toughness, is a major deficiency that significantly reduced the ductility of pre-Northridge moment connections (Lu et al. 2000, Kim et al. 2008). Without replacing groove-welded joints in existing moment connections, strengthening the beam end or reducing beam strength by trimming beam flanges have been investigated as rehabilitation alternatives in the United States (Civjan and Engelhardt 1998, Uang et al. 2000). In some cases, the rehabilitation scheme requires reinforcement of the connection near the column face using a welded haunch or cover plates (Engelhardt and Sabol 1998, Uang et al. 2000, Yu et al. 2000, Kim et al. 2002a, and Chi et al. 2006). These reinforced connections have developed ductile seismic responses in the laboratory.

[a] Department of Civil Engineering, National Taiwan University, Taipei, Taiwan
[b] Department of Civil Engineering, National Chiao Tung University, Hsinchu, Taiwan

Earthquake Spectra, Volume 26, No. 4, pages 927–950, November 2010; © 2010, Earthquake Engineering Research Institute

In Japan, Korea, and Taiwan, cold-formed or built-up box columns with wide flange beams are typically used to resist seismic loads in steel moment-resisting frames. Many fractures were observed in welded moment connections during the 1995 Kobe earthquake (Nakashima et al. 1998, 2000). Fractures occurred in welded metals, heat-affected zones, base metals (initiated from the toe of the beam weld access holes), and diaphragm plates. Moreover, connections damaged by the Northridge earthquake had no evidence of plastic deformation, but some connections damaged by the Kobe earthquake had significant plastic deformation prior to fracture. The major difference in connection behaviors results from different construction and fabrication practices in the United States and Japan. Japanese connections have the following characteristics: (1) two diaphragm plates are inserted between three separate column pieces and shop-welded all around using a complete joint penetration (CJP) groove weld, and (2) most beam flanges are groove-welded to the diaphragm plates using the YGW-11 electrode, which has CVN values exceeding 27 J at −29 °C, as specified in AISC seismic provisions (2005). Following the discovery of connection damage following the Kobe earthquake, most research focused on improving connection detailing such as the geometry of beam weld access holes, distance between the diaphragm-to-beam flange groove welds and the column face, and placement of backing bars and weld tabs. These minor modifications reflect the expectation that satisfactory performance of welded beam-to-column connections can be achieved using existing high-toughness weld metals.

The specific connection configuration in this study, which is commonly used in tall steel buildings in Japan (Nakashima et al. 2000), is motivated by construction and fabrication practices in Taiwan. A built-up box column requires extensive fabrication due to the longitudinal and internal diaphragm plate welds. This shop welding is completed under ideal conditions. Beam-to-column connections, similar to those used in the United States (i.e., beam flanges field-welded to the column and bolted beam web), are employed with the exception that a high-toughness electrode (i.e., E71T-1, ER70S-G or ER70S-6) is utilized. The connection performs better (i.e., 3% drift) than the pre-Northridge moment connections utilizing the E70T-4 electrode. However, the connection does not meet performance requirements based on AISC (2005) or *FEMA 350* (2000). Four internal flange stiffeners (IFSs), each of which is a rectangular flat plate, are welded to the column face and beam flange inner side to increase connection performance, such that it meets AISC (2005) seismic requirements. The proposed scheme (Chou et al. 2006, Jao 2007) differs from that utilizing the side plate connection (*FEMA 350* 2000), which completely eliminates reliance on existing beam flange groove-welded joints at the column face that transfer beam moments due to extremely poor ductility. All rehabilitation work proposed in this study is conducted within the beam flanges, such that the existing composite slab is not damaged and no additional requirements exist for story height. The goal of the study is to examine an alternative reinforcement technique to improve fracture resistance by strengthening connections already constructed with fracture resistance. Thus, the weld access hole in a beam web or backing bars is not modified, as suggested by Nakashima et al. (1998), for comparison.

In total, six large exterior moment connection specimens were tested. Two steel moment connections with bolted web-welded flanges were removed from an existing steel

building constructed prior to 1996; one connection was tested as a performance benchmark for non-rehabilitated moment connections in Taiwan. Note that this non-rehabilitated specimen was not used to replicate conditions existing in pre-Northridge moment connections in the United States. Rather, the intent was to start with a connection that was constructed according to Taiwanese fabrication practices. Rehabilitated moment connections with different internal flange stiffeners (IFSs) were tested to validate their cyclic performance. When reinforcement was sufficient, the rehabilitated connections, even those tested twice with a drift exceeding 4%, performed much better than non-rehabilitated connections, which failed due to welded joint fractures at the beam-to-column interface. This study experimentally and analytically assesses the cyclic behavior of the proposed moment connections, and provides recommendations for seismic design of such connections. Although the specific connection geometries may not be representative of practices in other countries, they still provide valuable information to understand the force transfer mechanisms in connections and fracture limit states.

REHABILITATED CONNECTION

CONNECTION DESIGN

Figure 1 shows a rehabilitated moment connection with IFSs. The IFSs are used to transfer some beam flange force to a column to reduce beam flange strain and prevent fracture of flange groove welds. A plastic hinge is assumed here to be located at one-quarter beam depth from the IFS end. This location, verified by Chou et al. (2010), conforms to *FEMA 350* (2000) recommendation for connections reinforced with either cover plates or welded haunches. The moment at the column face, determined by projecting moment capacity M_{PH} at the plastic hinge section, is

$$M_{dem} = \frac{L_b}{L_b - (L_s + d_b/4)} M_{PH} = \frac{L_b}{L_b - (L_s + d_b/4)} (\beta R_y \sigma_{yn} Z_b) \tag{1}$$

where L_b is the distance from the actuator to the column face; L_s is the IFS length; d_b is the beam depth; Z_b is the plastic section modulus of the beam; σ_{yn} is the specified yield strength of steel; R_y is the material over-strength coefficient, and coefficient β accounts for strain hardening (*FEMA 350* 2000). Since steel properties were obtained from tensile coupon tests before fabricating the specimens, actual yield strength, tensile strength, and $R_y = 1$ were used in Equation 1 to estimate moment demand.

Moment capacity near the beam-to-column interface increases due to presence of IFSs. The actual state of beam flexural stresses near the column face is complex, and may not be accurately predicted by a bending theory. It is assumed that full plastification can be developed in the beam and the IFS at high levels of interstory drift. Hence, the flexural capacity of the rehabilitated beam, M_{cap}, is the sum of beam flexural strengths, M_{pb} $(= Z_b R_y \sigma_{yn})$, and those of the IFSs, M_{ps}:

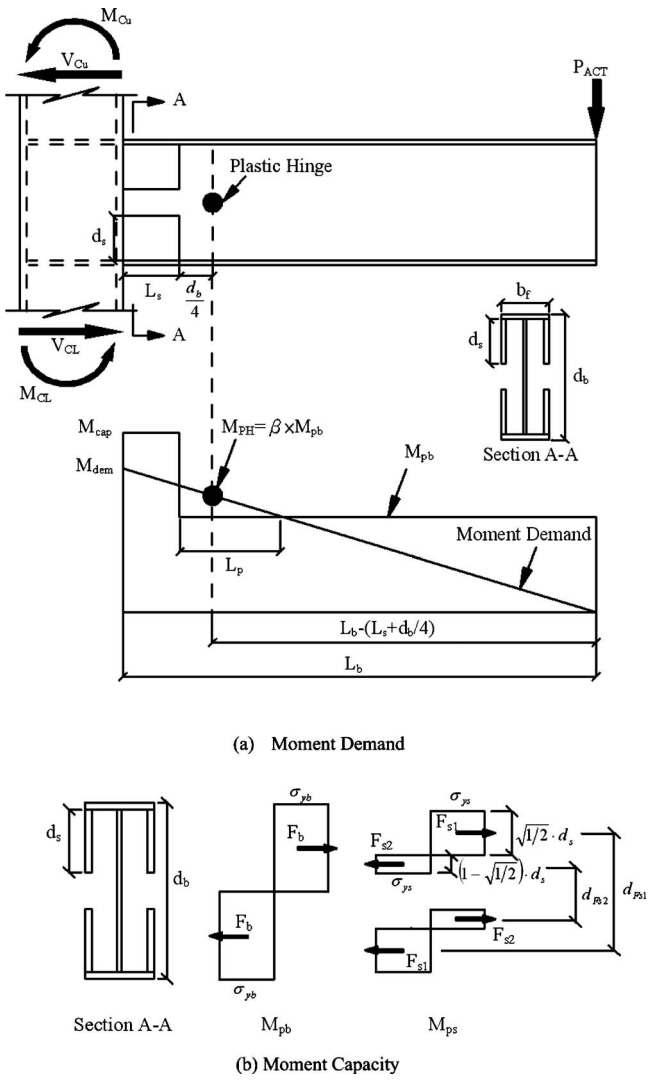

Figure 1. Moment capacity and demand of the beam.

$$M_{ps} = 2(F_{s1}d_{Fs1} - F_{s2}d_{Fs2}) = 2\left[R_y\sigma_{yn}\sqrt{\frac{1}{2}}d_s t_s\left(d_b - 2t_f - \sqrt{\frac{1}{2}}d_s\right)\right.$$
$$\left. - R_y\sigma_{yn}\left(1 - \sqrt{\frac{1}{2}}\right)d_s t_s\left(d_b - 2t_f - \left(1 + \sqrt{\frac{1}{2}}\right)d_s\right)\right]$$
$$= 2\left(2\sqrt{\frac{1}{2}} - 1\right)(d_b - 2t_f)R_y\sigma_{yn}d_s t_s \tag{2}$$

where t_f is the beam flange thickness; d_s is the IFS depth; t_s is the IFS thickness; F_{s1} and F_{s2} are the forces in the IFSs (Figure 1b), and d_{Fs1} and d_{Fs2} are the distances for each force couple in the IFSs. Because only one side of the IFS is connected to the beam flange and column (Figure 1a), the location of neutral axis in the IFS, developed from force equilibrium, varies from $2d_s/3$ in the elastic state to $\sqrt{1/2}d_s$ in the fully plastic state. Assuming that a moment capacity-demand ratio, $\alpha(=M_{cap}/M_{dem})$, in the rehabilitated beam exceeds 1, the IFS size can be determined from:

$$d_s t_s \geq \frac{\alpha M_{dem} - M_{pb}}{2\left(2\sqrt{\frac{1}{2}} - 1\right)(d_b - 2t_f)R_y\sigma_{yn}} \tag{3}$$

Since the force in the IFS $(=F_{s1}-F_{s2})$ is transferred to the beam via groove-welded joints, the length of the IFS, L_s, is determined as:

$$L_s \geq \frac{F_{s1} - F_{s2}}{0.9(0.6R_y\sigma_{yn})t_s} = \frac{\left(2\sqrt{\frac{1}{2}} - 1\right)R_y\sigma_{yn}t_s d_s}{0.9(0.6R_y\sigma_{yn})t_s} = 0.77d_s \tag{4}$$

When the moment capacities, M_{cap} and M_{pb}, moment demand, M_{dem}, and the IFS size are known, beam yield length, L_p, can be determined based on the geometrical relationship in Figure 1a.

The IFSs help transfer some beam moments to the column because existing beam flange groove-welded joints can sustain modest inelastic deformation before fracturing (Tsai et al. 1995, Chen et al. 2005, Chou et al. 2006). Existing groove welds of the beam top and bottom flanges do not need to be modified, indicating that the composite slab is not damaged. To verify the effects of IFSs on connection performance, a test program was conducted using full-scale beams and columns typically used in fabrication practices in Taiwan.

TEST PROGRAM

SPECIMENS

The experimental program consisted of tests of six specimens. Each specimen represented an exterior moment connection with one steel beam (H702 × 254 × 16 × 28) welded to a box column. Table 1 shows the columns and IFS sizes. The column and IFS were made of ASTM A572 Grade 50 steel, and the beam was made of ASTM A36 steel (Table 1). These two steels were manufactured in Taiwan and conform to the chemical and mechanical properties based on ASTM standards (1988). All connections were welded using the ER70S-6 electrode, which is similar to the E71T-8 and E70TG-K2 electrodes and provides a minimum specified Charpy V-Notch value of 27 J at −29 °C (20 ft-lbs at −20 °F). Beam-to-column groove welds in Specimens UR (Figure 2a) and IFS1 (Figure 2b) were made before 1996. The steel backing bars projected 50 mm beyond both sides of the beam flange, and the weld tabs were attached next to the beam flanges. Each pass of the flange groove welds was initiated and terminated when possible at a point outside the flange. This process

Table 1. Member sizes and properties

Spe. No.	Column Size	Column Stress σ_y[a] (MPa)	Column Stress σ_u[b] (MPa)	Beam Flange Stress σ_y (MPa)	Beam Flange Stress σ_u (MPa)	Beam Web Stress σ_y (MPa)	Beam Web Stress σ_u (MPa)	IFS Size ($t_s \times d_s \times L_s$)	IFS Stress σ_y (MPa)	IFS Stress σ_u (MPa)
UR	700×700×35×35	391	525	275	485	288	495	—	—	—
IFS1	700×700×35×35	391	525	330	—	320	—	22×175×300	370	500
IFS2	700×700×35×35	391	525	275	485	288	495	22×175×300	391	525
IFS3	550×550×35×35	385	530	285	440	280	435	22×175×300	370	500
IFS4	550×550×35×35	385	530	287	441	281	434	28×175×300	368	520
IFS5	550×550×35×35	385	530	285	440	280	435	22×308×300	371	500

[a] Actual yield strength;
[b] Actual tensile strength

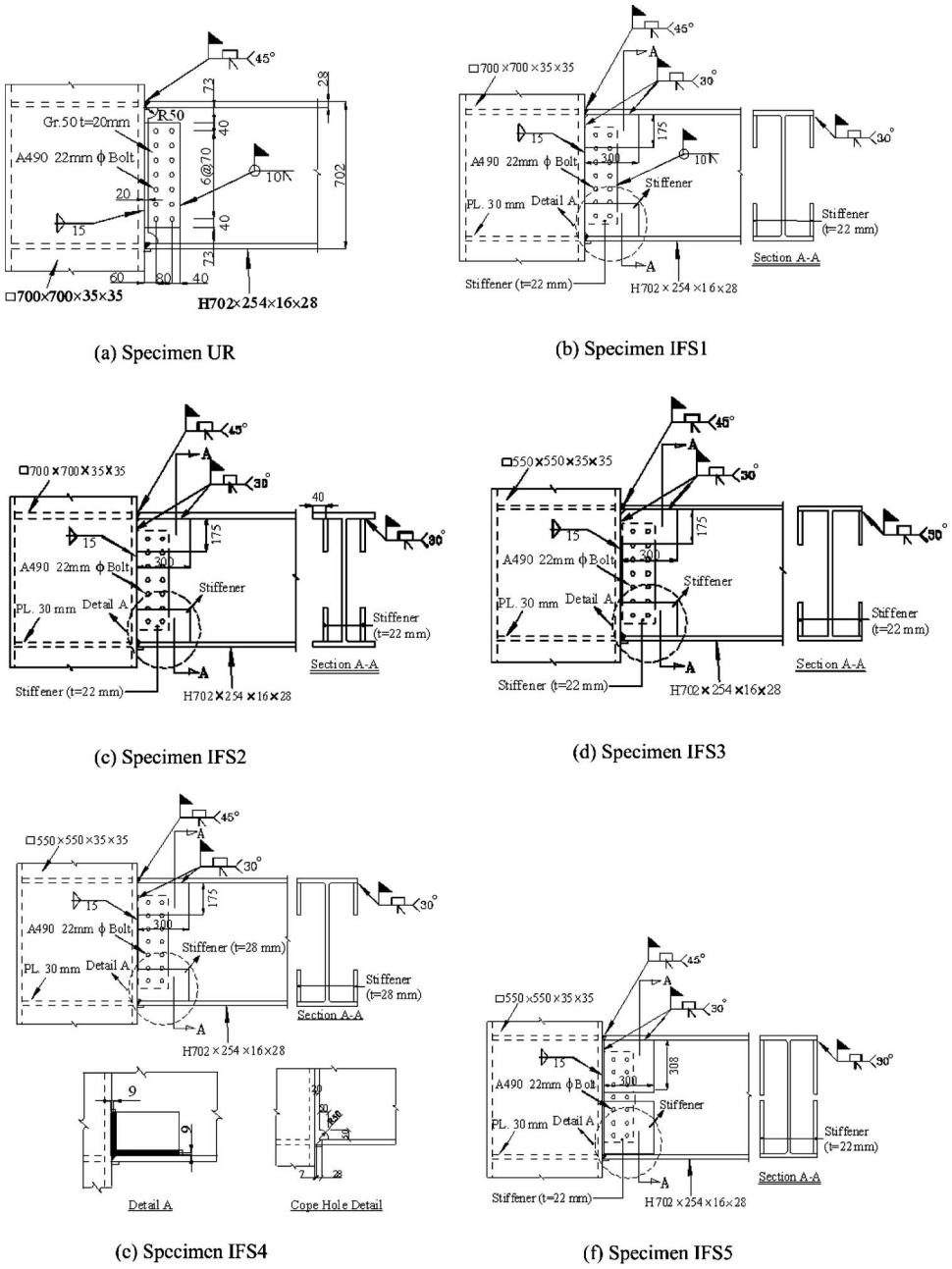

Figure 2. Connection details.

prevented poor-quality welds, which normally occur where a weld is started, on the beam flange-to-column face. In addition to a bolted web, supplemental fillet welds were used be-

Table 2. Beam moment capacity-demand ratios after rehabilitation

Specimen No.	β	M_{pb}	M_{PH}	M_{ps} (kN-m)	M_{dem}	M_{cap}	α	$\tilde{\alpha}$[a]
IFS1	1.2	2133	2560	762	2958	2895	0.98	—
IFS2	1.38	1800	2484	805	2870	2605	0.91	—
IFS3	1.27	1834	2329	762	2683	2596	0.97	—
IFS4	1.27	1845	2343	965	2697	2810	1.04	1.0
IFS5	1.27	1834	2329	1345	2683	3179	1.19	1.1

[a] Moment demand is calculated based on the actuator force at an interstory drift of 4%.

tween the shear tab and beam web. Four IFSs were welded to Specimen IFS1 (Figure 2b) in the laboratory after this specimen was removed from the existing building. Lab welds for Specimens IFS2-5 (Figures 2c–2f) were made by a fabrication shop welder, using weld positions typical of shop welding. Specifically, beam flange groove welds were made with the specimen oriented such that flat position welding was possible. Backing bars, which were about 60 mm wider than beam flange width, remained in place after welding, and no weld tabs were used. Each pass of the IFS-to-column groove welds was conducted before each pass of the IFS-to-beam groove welds. Specimens IFS2-5 did not have a fillet weld between the shear plate and beam web. For all specimens, the steel backing bar was left in place and a fillet weld, which can reduce the notch effect of a backing bar left in place, was not made between the backing bar and column.

Specimens IFS1-3 were retrofits of Specimen UR using the same IFS (Table 1). Specimen IFS2 was identical to Specimen IFS1, except that (1) the IFSs were located at the beam flange edges in Specimen IFS1 (Figure 2b) and 40 mm from the beam flange edges in Specimen IFS2 (Figure 2c), and (2) beam-to-column groove welds in Specimens IFS1 and IFS2 were made in the existing building prior to 1996 and in the laboratory in 2006, respectively. Specimen IFS3 was identical to Specimen IFS1, except that Specimen IFS3 had a smaller column (Table 1). The effects of distance from the IFS to the box column side plate were evaluated. Specimens IFS4 (Figure 2e) and IFS5 (Figure 2f) were identical to Specimen IFS3 (Figure 2d) except for IFS size (Table 1). In other words, the beam moment capacity-demand ratio, α ($=M_{cap}/M_{dem}$), was varied to study the effects of reinforcement on connection behavior. Table 2 lists information for beam moment capacity and demand and values of α and β. Notably, Specimens IFS1-3 have α values <1, indicating insufficient reinforcement compared to that of Specimens IFS4 and IFS5. The objective is to discover possible failure modes for rehabilitated connections.

TEST SETUP AND LOADING PROTOCOL

The connection specimens were tested (Figure 3). Restraint to lateral torsional buckling of the beam was provided near the actuator and at a distance of 1000 mm from the column face. Displacements were imposed on the beam by a 1000-kN actuator at a distance of 3875 mm from the column centerline. The AISC cyclic displacement history (2005) was used and run under displacement control. The interstory drift, which was computed by di-

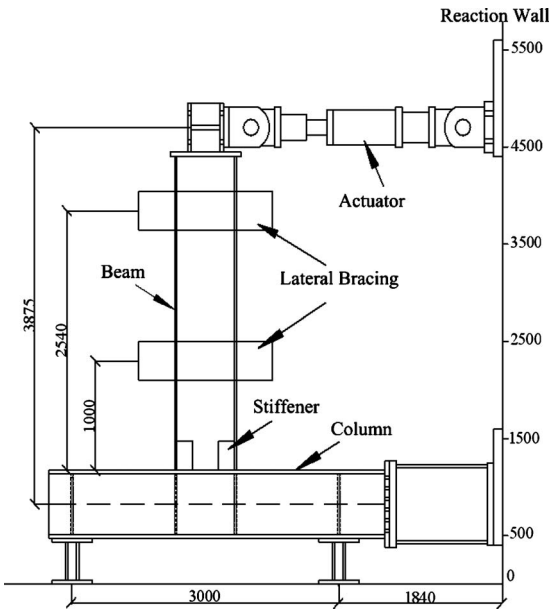

Figure 3. Test setup (unit: mm).

viding the actuator displacement by the distance to the column centerline, was used as a control variable. Specimens were tested until connection failure occurred or test limitations were reached.

TEST RESULTS

NON-REHABILITATED MOMENT CONNECTION

Figure 4a shows the global response of Specimen UR; the moment computed at the column face was normalized by the nominal plastic moment of the beam, M_{np} ($=Z_b\sigma_{yn}$). Whitewash flaking was observed in the beam flange at an interstory drift of 0.75%, indicating beam yield. At an interstory drift of 3%, minor fractures were observed in groove welds of the beam top flange and fillet welds of the shear plate to the column face. However, the peak strength was maintained at this drift level. A significant reduction in strength occurred toward an interstory drift of 4% due to fracture of the beam top flange (Figure 5). The column or panel zone did not yield throughout the test. The performance of Specimen UR exceeded drift demands from inelastic time history analyses of the existing building, but violated the requirements of AISC (2005) seismic provisions (Weng et al. 2009, Chou et al. 2010).

REHABILITATED MOMENT CONNECTION

Of the five rehabilitated specimens tested, Specimens IFS1-3 performed poorly, exhibiting brittle groove-weld failures at an interstory drift of 3%. Specimens IFS4 and

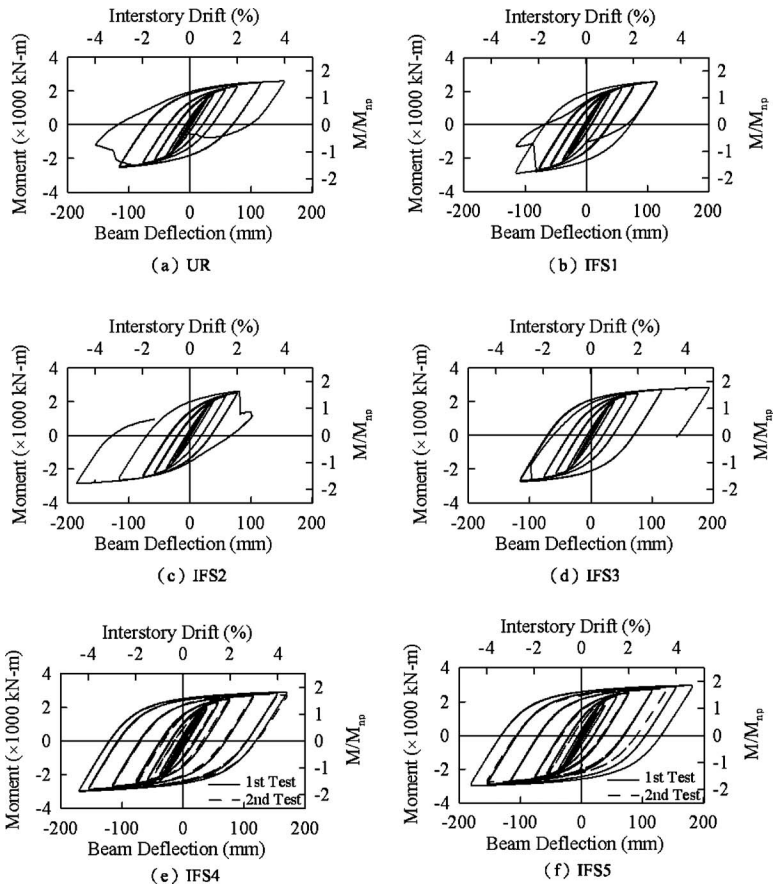

Figure 4. Beam moment-deflection responses.

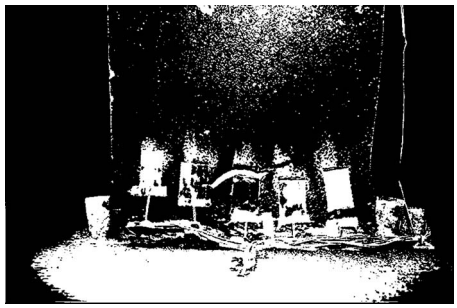

Figure 5. Beam top flange fracture of Specimen UR.

(a) Specimen IFS1 (Top Flange)

(b) Specimen IFS2 (Bottom Flange)

Figure 6. Specimens IFS1 and IFS2 weld fractures.

IFS5 were tested twice and performed extremely well, achieving high levels of interstory drift with no fractures of welded joints. The typical response of failed specimens is described, followed by a description of successful specimens.

Failed Specimens

Figures 4b and 4d show the hysteretic responses of Specimens IFS1 and IFS3, respectively. These two specimens sustained inelastic cycles of loading up to a 3% drift before a brittle fracture occurred in the top flange weld. The fracture passed completely through the groove-welded metal connecting the top flange to the column (Figure 6a). Specimen IFS2 had a brittle fracture in the bottom flange weld, causing complete separation of the beam bottom flange from the column face (Figure 6b). Further investigation after the beam was removed from the column indicated that the fracture was within the

column face, immediately adjacent to the groove weld. Specimens IFS1 and IFS2 had a similar deformation capacity irrespective of whether the flange groove welds were made in the field or laboratory. This finding suggests that using high-toughness electrodes is highly beneficial to connection behavior. Even when toughness is reduced due to improper welding conditions (field versus laboratory), a very high level of toughness can remain. However, such a connection still fails to satisfy the stringent AISC seismic provisions (2005). These specimen failures suggest that reinforcement, which corresponds to low beam capacity-demand ratios (Table 2), does not reduce the stress concentration in groove welds, and considerable reinforcement is needed to improve connection behavior.

Successful Specimens

Specimens IFS4 and IFS5 were identical to Specimen IFS3, except that (1) the IFS thickness of 22 mm of Specimen IFS3 was increased to 28 mm in Specimen IFS4, and (2) the IFS depth of 175 mm of Specimen IFS3 was increased to 308 mm in Specimen IFS5. Specimens IFS4 and IFS5 had beam capacity-demand ratios of 1.04 and 1.19, respectively, larger than those of failed specimens, and each specimen had similar patterns of improved behavior. Yielding, observed by whitewash flaking, occurred at an interstory drift of 0.75%, concentrated within the beam flange region roughly 400 mm from the column face. After finishing the 4% drift cycles, yield extended more than 1000 mm from the column face without any signs of flange or web buckling. For subsequent loading cycles, Specimens IFS4 and IFS5 achieved maximum interstory drifts of 4.4% and 4.7%, respectively, with minor beam buckling. The flange and web buckling amplitudes, measured at a distance of 220 mm from the IFS end, were about 2 mm and 7 mm, respectively, in Specimen IFS4 (Figure 7a), and about 8 mm and 18 mm, respectively, in Specimen IFS5. The maximum moment developed at the assumed plastic hinge location was 1.3–1.4 times the actual plastic moment of the beam; the value of strain hardening exceeded 1.27 when calculated based on *FEMA* 350 (Table 2).

Since beam local buckling was minor and no strength degradation was observed after the first cyclic test, Specimens IFS4 and IFS5 were retested using the same AISC loading protocol (2005). The hysteretic responses in the first and second tests were similar (Figures 4e and 4f). However, at an interstory drift of 3%, beam local buckling accompanied by beam twisting caused a small reduction in beam flexural strength for both specimens. At the end of the second test for Specimen IFS4 (4.4% drift), flange and web buckling amplitudes increased to 27 mm and 52 mm (Figure 7b), respectively, reducing strength by 6% compared with that in the first test (Figure 4e). Because beam residual deformation of Specimen IFS5 was large after the first test, this specimen was re-loaded to an interstory drift between −4 and 3.6%. A minor tearing of the beam flange at the end of the stiffener was observed at an interstory drift of 2%. However, this tearing (Figure 8a), caused by flange local buckling, had no adverse effect on specimen strength throughout the second test. Figure 8b shows the yielding and buckling pattern of Specimen IFS5 after the second test; flange and web buckling amplitudes were 21 mm and 32 mm, respectively. The hysteretic loop had a slight reduction in strength (Figure 4f).

(a) First Test

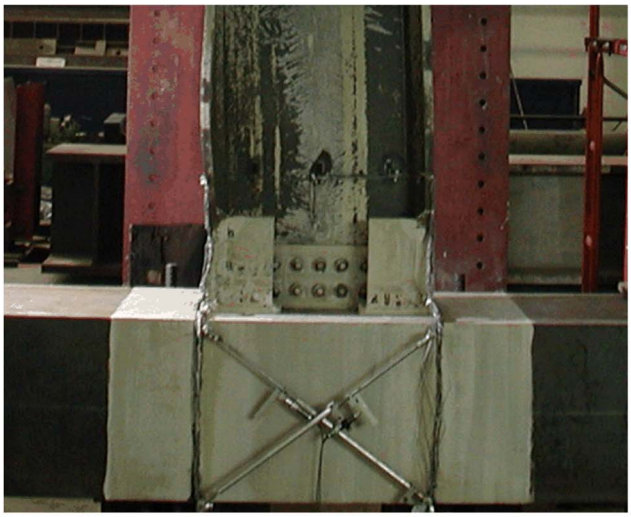

(b) Second Test

Figure 7. Yielding and buckling in Specimen IFS4 (4.4% drift).

BEAM FLANGE STRAINS

The ability of the IFS to decrease beam flange tensile strain was observed from measured strains at 60 mm from the column face (Figure 9). At an interstory drift of 3%, tensile strains in the beam bottom flange of non-rehabilitated Specimen UR were in the range of 2–3%, much higher than those of rehabilitated specimens. The tensile strains in Specimen IFS3 were lower than those in Specimen IFS1, suggesting that the IFS located close to the side plate of the welded box column effectively reduced tensile strain. Furthermore, failed

(a) Crack at IFS End

(b) Buckling Pattern

Figure 8. Specimen IFS5 after second test.

Specimens IFS1 and IFS3 had higher tensile strains than successful Specimens IFS4 and IFS5, indicating that the IFS with adequate strength and stiffness effectively reduced strains and thereby prevented flange groove-weld fracture. Maximum tensile strain for successful Specimens IFS4 and IFS5 at an interstory drift of 4% was about 0.8%, equaling $5.6\varepsilon_y$, where ε_y is yield strain.

Flange strain along the beam axis of Specimen IFS5 was highest beyond the IFS (Figure 10). At an interstory drift of 4%, maximum strain (gage S16) at the assumed location of the beam plastic hinge was about $16\varepsilon_y$ in tension (Figure 10c) and $13\varepsilon_y$ in compression (Figure 10d), demonstrating successful relocation of the plastic hinge from the column face.

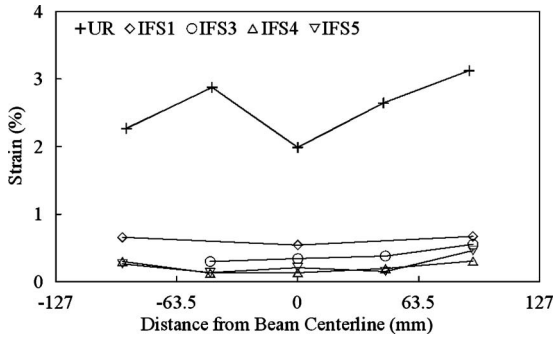

Figure 9. Strain profiles across the beam bottom flange width (3% drift).

INTERNAL FLANGE STIFFENER STRAINS

Figure 11 presents the measured longitudinal strains along the stiffener depth, 35 mm from the column face. Longitudinal strains beyond the neutral axis of the IFS have values that are opposite those of the side of the IFS connecting the beam flange, and longitudinal strains near the beam flange are greater than yield strain. Because Specimen IFS3 has weaker stiffeners than Specimens IFS4 and IFS5, tensile strain of the IFS near the beam bottom flange of Specimen IFS3 is highest among these specimens. For Specimen IFS2, in which the stiffener is located far from the box column side plate, the stiffener shows low

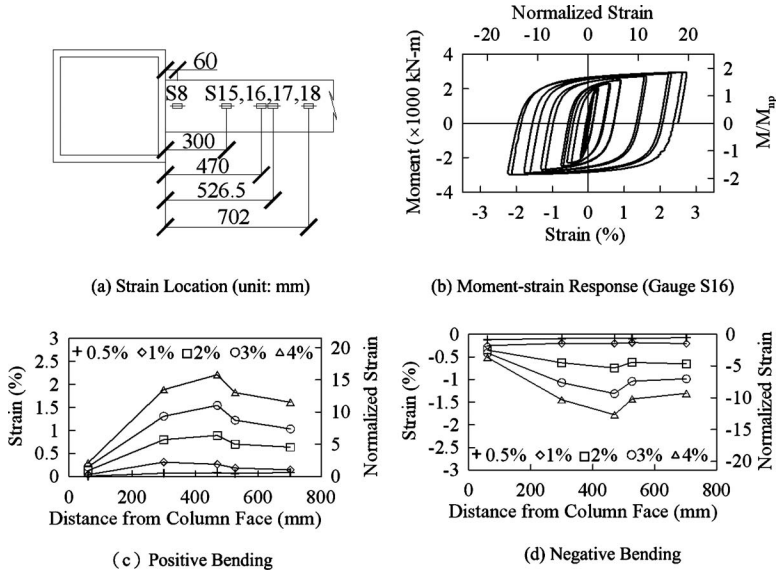

Figure 10. Bottom flange strain profiles along a beam axis (Specimen IFS5).

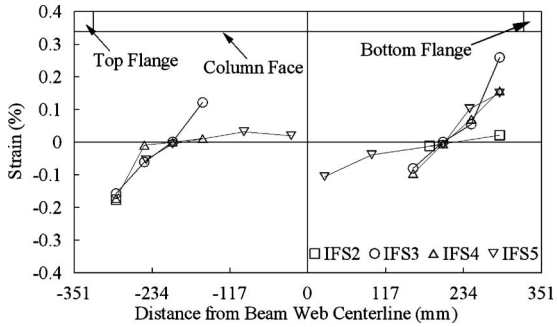

Figure 11. IFS strain profiles (beam positive bending at a 2% drift).

tensile strain, indicating poor efficiency. The maximum tensile strains measured at an interstory drift of 4% were roughly $2.4\varepsilon_y$ for Specimen IFS4 and $2.2\varepsilon_y$ for Specimen IFS5.

ANALYTICAL STUDY

The finite element models were prepared for Specimens UR, IFS3, IFS4, and IFS5 using the finite element analysis program ABAQUS (2003) to investigate potential sources of failure mode. Figure 12a shows the finite element model, which consists of eight-node brick elements that use standard integration. The groove welds joining the beam flange and column (Figure 12b) and joining the stiffener to the column and beam flange (Figure 12c) were modeled. The geometry of beam flange groove welds was considered based on flange bevel angle and the gap between the beam flange and column. The geometry of IFS groove welds was also considered based on IFS bevel angle and the gap between the beam flange and column. The steel backing and weld access hole were not modeled. Coordinates common to components joined by the shear tab and beam web were constrained, such that they had identical displacements. Material properties used for the models were obtained from tensile coupon tests (Table 1). The yield and tensile strengths of the weld metal obtained from the fabricator were 469 MPa and 563 MPa, respectively; the stress-strain curve was approximated by using a bi-linear relationship. No residual stresses of groove welds were taken into account in the modeling. Analyses accounted for material nonlinearities, using the von Mises yield criterion. Combined isotropic and kinematic hardening was assumed for cyclic analysis; modeling parameters were obtained from the study by Chou and Wu (2007). Since beam buckling was minimal in the first test (Figure 4), it was not considered in analysis.

Figure 13 shows comparisons of beam moment-deflection hysteretic responses, longitudinal strains in the beam flange and the IFS from the test and analysis. Both initial stiffness and post-yield results are in good agreement with test data (Figure 13a). The longitudinal strains in the beam flange (Figure 13b) and IFS (Figure 13c), which are obtained near the column face in the finite element model, also correlate well with test data. Moment, M_s, transferred through the IFS to the column was computed from longitudinal stresses along the IFS depth, the respective cross-sectional area, and distance

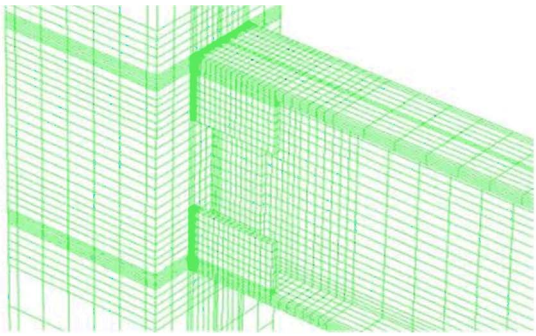

(a) Global Model

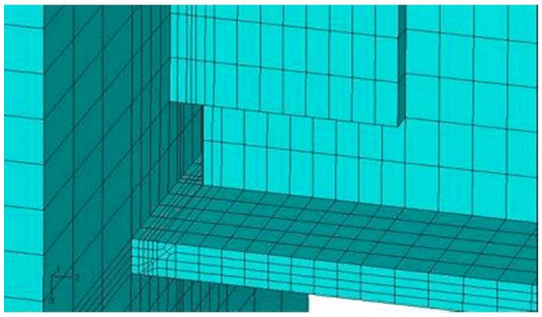

(b) Beam-to-Column Interface

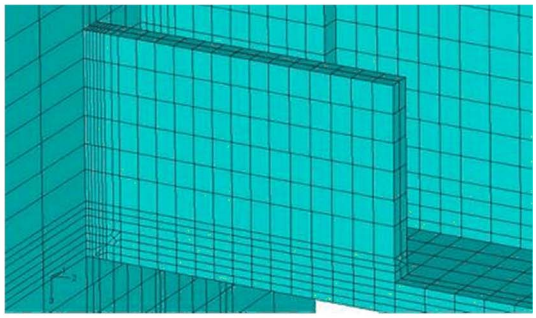

(c) Stiffener to Beam Flange and Column

Figure 12. Finite element model.

to the beam web centerline. The ratio of M_s to the connection moment, M_{ABA}, computed at the column face increased as drift increased (Figure 14). Specimens IFS4 and IFS5 had higher moment resistance of the IFS than failed Specimen IFS3, indicating that a stiffener

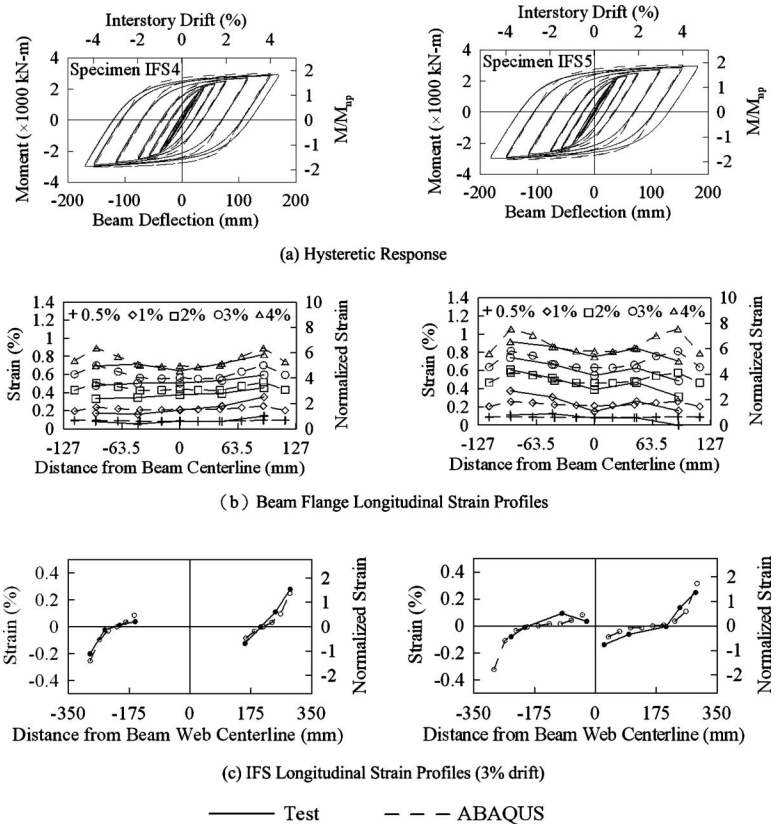

Figure 13. Comparison between test and ABAQUS results.

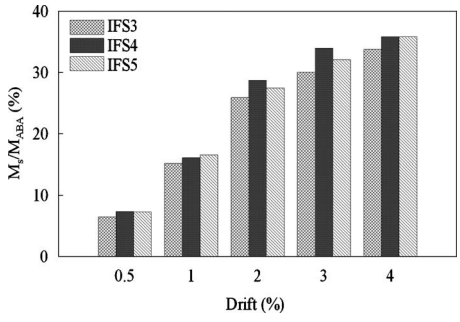

Figure 14. IFS moment contribution ratio (positive bending).

with increased thickness or depth helps transfer a large moment from the beam flange to the column. This moment ratio was about 35% for a successful specimen at an interstory drift of 4%.

The rupture index (RI) was computed at different connection locations to identify possible fracture sources. The same approach was used by other analytical connection studies (Mao et al. 2001, Kim et al. 2002b). The RI equals the product of a material constant and the plastic equivalent strain (PEEQ) divided by strain at the ductile fracture, ε_r, which is derived by Hancock and Mackenzie (1976) as:

$$\mathrm{RI} = \frac{a\mathrm{PEEQ}}{\varepsilon_r} = \frac{\sqrt{\frac{2}{3}\varepsilon_{ij}^{p}\varepsilon_{ij}^{p}}\Big/\varepsilon_y}{\exp\left(-1.5\frac{\sigma_m}{\sigma_{eff}}\right)} \tag{5}$$

where ε_{ij}^{p} represents the plastic strain components; σ_m is the hydrostatic stress, and σ_{eff} is the von Mises stress. Therefore, locations in a connection with high RI values have high fracture potential. Figure 15a presents data for RI distributions at three locations–the beam flange top surface located 60 mm from the column face (Line A), the groove-welded top surface near the column face (Line B), and the beam flange inner side along the welds between the IFS and beam flange (Line C). The RI values can be significantly reduced at the beam flange near the column face with an IFS (Figure 15b). However, the maximum RI of rehabilitated specimens at both ends of the beam flange groove weld is higher than that of the non-rehabilitated specimen (Figure 15c). The RI at the IFS end also increases (Figure 15d), indicating that another possible fracture source exists in addition to that on the beam-to-column interface. Figure 15e shows the maximum RI for each specimen at the three locations. Specimens not rehabilitated have a maximum RI value in the beam flange near the groove weld (Line A), corresponding to a beam flange fracture during testing (Figure 5). The maximum RI value in rehabilitated specimens is lower than that in the non-rehabilitated specimen; however, the likely location of a fracture is at the beam-to-column interface (Line B), as evidenced by failed specimens (Figure 6). Specimen IFS4 with an IFS thickness equal to that of the beam flange is the best connection because the RI value at any location is lowest among all rehabilitated specimens. The maximum RI is 1.1 (Figure 15c) when a fracture occurs along Line B in the Specimen IFS3 test.

This work also examines the influence of IFS size on RI distributions at the likely fracture location (Line B). Eighteen different IFSs (Table 3) were selected to reinforce the connection of Specimen IFS3. The material properties of the IFS in Specimen IFS3 were used in analyses. The beam capacity-demand ratios, α, of these models were 0.93–1.27 (Table 3). Figure 16 shows the maximum RI on Line B for each model subjected to AISC cyclic loading (2005); the RI variation is inversely dependent on stiffener thickness, t_s, and weakly dependent on stiffener length, L_s. Notably, a stiffener with a large d_s can reduce RI values.

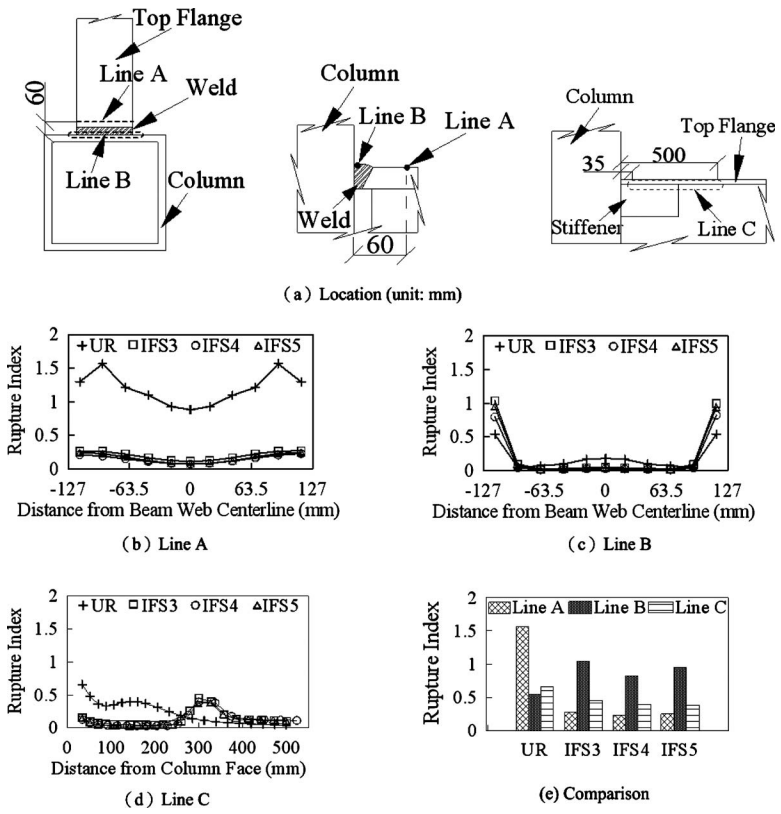

Figure 15. Rupture index (RI) comparison at a 3% drift.

Table 3. Values of α in finite element models with different IFSs

		t_s (mm)	
L_s (mm)	d_s (mm)	22	28
208	175	0.93	1.01
	245	1.04	1.14
	308	1.14	1.27
254	175	0.92	0.99
	245	1.03	1.13
	308	1.12	1.25
300	175	0.90	0.98
	245	1.01	1.11
	308	1.11	1.23

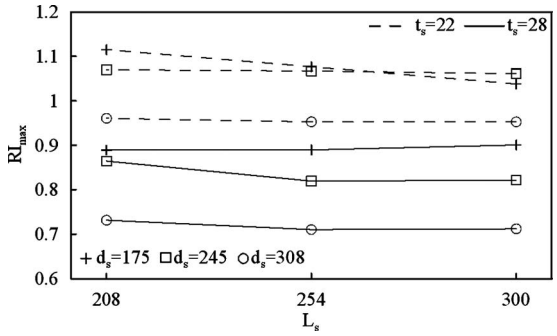

Figure 16. Maximum RI values on line B (3% drift).

SUMMARY OF THE REHABILITATED CONNECTION DESIGN PROCEDURE

A design procedure for the seismic rehabilitation of a bolted web-welded flange moment connection is proposed based on experimental and analytical results. The details of a non-rehabilitated fully restrained moment connection are as follows: (1) beam flange groove welds are made using an electrode with high notch toughness (i.e., ER70S-6, E71T-8, or E70TG-K2 electrodes) with steel backing bars left in place; (2) the beam web is bolted to the column shear plate without supplemental fillet welds between the shear plate and beam web; and (3) continuity plates in the box column are as thick as the beam flange. The step-by-step design procedure is as follows:

Step 1: Select IFS length, L_s.

Step 2: Compute the beam plastic moment at the column face, M_{dem}, using a strain hardening factor, β, of 1.3–1.4 for this specific connection (Equation 1).

Step 3: Use Equation 3 to determine IFS size with a rehabilitated beam moment capacity-demand ratio, α, of 1.0–1.1.

Step 4: Check IFS length using Equation 4. Iterate over a new L_s by returning to Step 1 when Equation 4 is not satisfied.

CONCLUSIONS

Six large exterior moment connection specimens, each composed of an ASTM A572 Grade 50 welded box column and an ASTM A36 H702 × 254 × 16 × 28 beam, were tested and analyzed to verify the proposed rehabilitation scheme. Five specimens were reinforced with different IFSs, which were groove welded to the column face and inner side of the beam flange. The ER70S-6 electrode, which is similar to the E71T-8 or E70TG-K2 electrodes, was used to make beam flange groove welds in all specimens based on typical construction practices in Taiwan. The modification scheme does not require removal of steel backing bars of the top and bottom flanges and no fillet welds were made between the steel backing bar and column face. Web joints were made with slip-critical, high-strength bolts connecting the beam web to a shear tab welded to the column face. Finite element models of

four specimens were generated using solid elements to verify IFS effectiveness and identify possible failure sources. The following conclusions are based on experimental results and associated analyses.

1. Specimen UR without rehabilitation was removed from an existing steel building constructed prior to 1996. Although this specimen utilized an ASTM A36 beam, high-toughness flange groove welds, and fillet welds between the shear tab and beam web in addition to slip-critical bolts, brittle fracture of the beam flange occurred before reaching an interstory drift of 4%, not satisfying AISC (2005) seismic requirements.
2. The capacity design procedure was adopted to design rehabilitated specimens with IFSs. The flexural capacity of the rehabilitated beam was the sum of plastic moments of a non-rehabilitated beam and four IFSs. Because the IFS was subjected to eccentric loading from welded joints, the IFS had tensile and compressive stresses along the stiffener depth.
3. Maximum moment developed at one-quarter beam depth from the IFS end was 1.3–1.4 times the actual plastic moment of the beam. The 1.3–1.4 factor accounted for strain hardening that was accompanied by large inelastic deformations with minor beam buckling; this value was higher than that calculated based on *FEMA 350* (2000).
4. Two successful rehabilitated specimens, which had beam capacity-demand ratios exceeding 1, had very minor beam local buckling after the first AISC cyclic loading test with a drift in excess of 4%. These specimens had no brittle fractures of the beam flange groove-welded joint, even after the second loading test to a drift of 4%. However, a minor strength reduction was due to beam buckling in the second test. Although the IFS did not eliminate inelastic straining near the beam-to-column face, such modest strains (about 5–6 times yield strain) had no deleterious effects on the response of successful specimens. However, the IFS did not prevent brittle fractures of groove-welded joints on the three rehabilitated specimens, which had beam capacity-demand ratios <1. Therefore, this ratio of 1.0–1.1 can be used as a minimum requirement for seismic design of this connection type.
5. Finite element analysis shows that the IFSs transferred about one-third of the connection moment to the column. The IFSs also effectively reduced RI demands on the beam flange and groove-welded joint of the beam flange excluding both ends. The high RI values at beam flange edges were evidence of fractures of the groove-welded joints in failed specimens with insufficient reinforcement. Parametric study shows that RI demand was effectively reduced by increasing IFS thickness or depth.

Although the proposed rehabilitation scheme improves the cyclic performance of welded beam-to-box column connections to satisfy AISC seismic provisions (2005), future study is needed to verify the feasibility of applying rehabilitated connections to wide-flange columns. The force transfer mechanism between the beam and IFSs should also be further examined.

REFERENCES

American Institute of Steel Construction (AISC), 2005. *Seismic Provisions for Structural Steel Buildings*, Chicago, IL.

American Society for Testing and Materials (ASTM), 1988. *Specification for Structural Steel*, Philadelphia, PA.

Chen, C. C., Chen, S. W., Chung, M. D., Lin, M. C., 2005. Cyclic behavior of unreinforced and rib-reinforced moment connections, *J. Constr. Steel Res.* **61**, 1–21.

Chi, B. C., Uang, C. M., Chen, A., 2006. Seismic rehabilitation of pre-northridge steel moment connections: a case study, *J. Constr. Steel Res.* **62**, 783–792.

Chou, C. C., Wu, C. C., Jao, C. K., and Wang, Y. Y., 2006. Weakened and strengthened steel moment connections, *4th International Conference on Earthquake Engineering*, Paper No: 152, Taipei Taiwan.

Chou, C. C., and Wu, C. C., 2007. Performance evaluation of steel reduced flange plate moment connections, *Earthq. Engrg. Struct. Dyn.* **36**, 2083–2097.

Chou, C. C., and Uang, C. M., 2007. Effects of continuity plate and transverse reinforcement on cyclic behavior of SRC moment connections, *J. Structural Engineering, ASCE* **133**, 96–104.

Chou, C. C., Weng, C. Y., and Chen, J. H., 2008. Seismic design and behavior of post-tensioned connections including effects of a composite slab, *Eng. Struct.* **30**, 3014–3023.

Chou, C. C., Tsai, K. C., Wang, Y. Y., and Jao, C. K., 2010. Seismic rehabilitation performance of steel side plate moment connections, *Earthquake Eng. Struct. Dyn.* **39**, 23–44.

Civjan, S., and Engelhardt, M. D., 1998. *Experimental Investigation of Methods to Retrofit Connections in Existing Seismic-Resistant Steel Moment Frames*, Summary Final Rep. to the National Institute of Standards and Technology, Phil M. Ferguson Struct. Engrg. Lab., University of Texas at Austin.

Engelhardt, M. D., and Sabol, T. A., 1998. Reinforcing of steel moment connections with cover plates: benefits and limitations, *Eng. Struct.* **20**, 510–520.

Federal Emergency Management Agency (FEMA 350), 2000. *Recommended Seismic Design Criteria for New Steel Moment-Frame Buildings, FEMA 350*, Federal Emergency Management Agency, Washington, D.C.

Hibbitt, Karlsson & Sorensen (ABAQUS), 2003. *ABAQUS User's Manual Version 6.3*, Pawtucket, RI.

Hancock, J. W., and Mackenzie, A. C., 1976. On the mechanism of ductile fracture in high-strength steel subjected to multi-axial stress states, *J. Mech. Phys. Solids* **24**, 147–169.

Jao, C. K., 2007. Seismic behavior of steel retrofitted moment connections with stiffeners inside beam flange, *Thesis advisor: Chou, C. C.*, National Chaio Tung University, Hsinchu, Taiwan. (in Chinese).

Kim, T., Whittaker, A. S., Gilani, A. S. J., Bertero, V. V., and Takhirov, S. M., 2002a. Experimental evaluation of plate-reinforced steel moment-resisting connections, *J. Struct. Engrg., ASCE* **128**, 483–491.

Kim, T., Whittaker, A. S., Gilani, A. S. J., Bertero, V. V., and Takhirov, S. M., 2002b. Cover-plate and flange-plate steel moment-resisting connections, *J. Struct. Engrg., ASCE* **128**, 474–482.

Kim, T., Stojadinovic, B., and Whittaker, A., 2008. Seismic performance of pre-Northridge welded steel moment connections to built-up box columns, *J. Struct. Engrg., ASCE* **134**, 289–299.

Lu, L. W., Ricles, J., Mao, C., and Fisher, J., 2000. Critical issues in achieving ductile behavior of welded moment connections, *J. Constr. Steel Res.* **55**, 325–341.

Mao, C., Ricles, J., Lu, L. W., and Fisher, J., 2001. Effect of local details on ductility of welded moment connections, *J. Struct. Engrg., ASCE* **127**, 1036–1044.

Nakashima, M., Suita, K., Morisako, K., and Maruoka, Y., 1998. Tests of welded beam-column subassemblies I: global behavior, *J. Struct. Engrg., ASCE* **124**, 1236–1244.

Nakashima, M., Roeder, C. W., and Maruoka, Y., 2000. Steel moment frames for earthquakes in Unites States and Japan, *J. Struct. Engrg., ASCE* **126**, 861–868.

Tsai, K. C., Wu, S., and Popov, E. P., 1995. Experimental performance of seismic steel beam-column moment joints, *J. Struct. Engrg., ASCE* **126**, 925–931.

Uang, C. M., Yu, Q. S., Noel, S., and Gross, J., 2000. Cyclic testing of steel moment connections rehabilitated with RBS or welded haunch, *J. Struct. Engrg., ASCE* **126**, 57–68.

Yu, Q. S., Uang, C. M., and Gross, J., 2000. Seismic rehabilitation of steel moment connections with welded haunch, *J. Struct. Engrg., ASCE* **126**, 69–78.

Weng, Y. T., Tsai, K. C., Chen, P. C., Chou, C. C., Chan, Y. R., Jhuang, S. J., and Wang, Y. Y., 2009. Seismic performance evaluation of a 34-story steel building retrofitted with response modification elements, *Earthq. Engrg. Struct. Dyn.* **38**, 759–781.

(Received 9 November 2007; accepted 2 April 2010)